Open Access Full Text Article

ORIGINAL RESEARCH

Multifunctional ROS-Responsive and TME-Modulated Lipid-Polymer Hybrid Nanoparticles for Enhanced Tumor Penetration

Rui Ni [1-3], Lele Huang[3], Zhen Li[4], Wenli Zhang[4], Yajie Wang[4], Yan Shen [4], Jianxin Wang[1], Weigen Lu[2]

[1]School of Pharmacy, Fudan University, Shanghai, People's Republic of China; [2]China State Institute of Pharmaceutical Industry, Shanghai, People's Republic of China; [3]National Advanced Medical Engineering Research Center, Shanghai, People's Republic of China; [4]Department of Pharmaceutics, China Pharmaceutical University, Nanjing, People's Republic of China

Correspondence: Jianxin Wang, School of Pharmacy, Fudan University, Shanghai, 201203, People's Republic of China, Email jxwang@shmu.edu.cn; Weigen Lu, China State Institute of Pharmaceutical Industry, Shanghai, 201203, People's Republic of China, Email sipiluwg@163.com

Purpose: To enhance tumor penetration by formulation design and tumor microenvironment (TME) modulation, herein a novel reactive oxygen species (ROS)-responsive size/shape transformable lipid-polymer hybrid nanoparticle (LPN) has been fabricated for the co-delivery of an anticancer and collagen-inhibition drug.

Methods: A ROS-responsive poly(D, L-lactide)-thioketal-polyethylene glycol (PLA-TK-PEG) co-polymer was synthesized. LPNs were then fabricated by encapsulation of losartan (LST)-loaded micelles as the core to support paclitaxel (PTX)-loaded liposomes. The PEG content in the lipid shell of LPNs was then adjusted to obtain the size-/shape-transformable LPNs (M/LST-Lip/PTX-PEG$_{5\%}$). The ROS-responsiveness was observed in vitro by transmission electron microscopy and the tumor-penetration of the LPNs was evaluated in 3D tumor spheroids by confocal laser scanning microscopy. Tumor-targeting, tumor-penetrating, and antitumor efficacies of the NPs in 4T1 tumor-bearing mice were determined by in vivo imaging.

Results: ROS-responsive micellar core degradation and the transformation of spherical LPNs (120nm) to smaller 40 mm discoid nanoparticles (NP) were observed. The transformable LPNs exhibited enhanced capacity of penetration in contrast to the un-transformable preparations in three-dimensional (3D) tumor spheroids. Furthermore, synergetic penetrating enhancement was achieved by LST-loaded transformable LPNs in 4T1 and fibroblast cell mixed 3D tumor spheroids. The improved tumor penetration of LST-loaded transformable LPNs was observed in vivo, which could be due to their collagen inhibiting and size/shape transformable effect. Due to their enhanced penetrability, LST and PTX-loaded transformable LPNs demonstrated significant in vivo antitumor efficacy in comparison to other preparations.

Conclusion: The results confirmed the efficacy of M/LST-Lip/PTX-PEG$_{5\%}$ in tumor targeting, collagen inhibition in TME, and enhanced tumor penetration. This novel drug delivery system can therefore play a substantial role in improving the therapeutic efficacy of antitumor drugs combined with TME-improving agents.

Keywords: lipid-polymer hybrid nanoparticles, losartan, paclitaxel, ROS responsiveness, drug delivery, collagen inhibition, tumor penetration, combination therapy

Introduction

In recent decades, nanoparticles (NPs) have been used extensively for tumor-targeted delivery of chemotherapy drugs with reduced adverse effects and enhanced bioavailability. However, the range of their therapeutic effects has been limited due to the inability of these nanomedicines to easily penetrate the physiological barriers of the tumor.[1] While the enhanced permeation and retention effect (EPR) promotes the extravasating of nanotherapeutics from the leaky regions of tumor vasculature, the dense collagen matrix of tumor microenvironment (TME) hinders them from further delivery, especially the ones with sizes >100 nm.[2–6] Therefore, adjustments of nanocarriers and TME are among the most significant strategies to optimize tumor penetration efficacy for NP delivery systems.

Tumor penetration of NPs is highly dependent on their physicochemical properties (particle size, shape, surface charge, etc), and regulating these factors has been shown to enhance tumor penetration.[7–12] For instance, NPs with smaller sizes tend to have deeper penetration, but undersized ones (<10nm) are susceptible to being removed by the reticuloendothelial system.[13] Particle size reduction acts as a brilliant strategy for the improvement of NP delivery by striking a proper balance between sufficient circulation time and penetration efficacy. In addition to controlling the size of NPs, changing their shape has also shown to play an increasingly important role in the improvement of targeted drug delivery.[14,15] Studies have shown that non-spherical NPs (such as rod, discoid, ellipsoid, etc.) may be more efficient in targeting tumors in comparison to spherical NPs. For instance, discoid-shaped NPs with low aspect ratios have been shown to exhibit the largest intra-tissue transmission and uniform penetration.[16,17] However, the oscillating trajectory of discoid-shaped NPs can affect the targeting efficiency as they can be easily ingested into the circulatory system due to increased opportunities for interaction with the vascular wall.[18,19] Therefore, shape/size adjustment can be a preferable strategy to enhance delivery efficiency of NPs.

TME stimuli such as low pH, overexpressed matrix metalloproteinase, and the presence of reactive oxygen species (ROS) are effective triggers for achieving the desired degree of transformation post its arrival at the tumor site.[20–23] Among these triggers, elevated expression of ROS has been detected within the tumor tissues, the concentration of which could be 2–5 times higher than that in normal tissues (50–100 $\mu mol \cdot L^{-1}$ vs 20 $nmol \cdot L^{-1}$). Many ROS-responsive polymers have been explored based on the elevated levels of ROS in tumor tissues and include ROS-sensitive groups such as sulfur, selenium, tellurium, unsaturated lipids, etc.

A new generation nano-delivery vehicle of lipid-polymer hybrid nanoparticles (LPNs) comprising a polymer core and a liposome shell with lipid-PEG, provides an opportunity to integrate the above-mentioned strategies to function in synchronized transformation of size and shape. It has been reported that a shape-transformation of liposome NPs from sphere to discoid with an increase in PEG content to a certain extent.[12] While the discoid liposome NPs could regain their spherical shape as long as a supportive spherical core was encapsulated.[24] Therefore, when the polymer core degrades in response to a certain biological trigger or expectant conditions, the liposome shell would shrink down to discoid particles of smaller size. Both the core and the shell could be designed to be loaded with therapeutic drugs leading to drug release and delivery during its transformation.

However, adjustments to the physicochemical properties of NPs have limited effects and cannot change the obstruction of tumor penetration by the microenvironment. Based on continuous in-depth investigations of the physiological characteristics of tumors, the TME has been shown to play an important role in the occurrence, development, metastasis, and relapse process of tumors. The regulation of TME has been investigated for the enhancement of the efficacy of anti-tumor drugs. In the current investigation, we have intended to use Losartan (LST) as a TME-modulator to assist Paclitaxel (PTX) which is an anti-tumor drug. LST is a common prescription drug with antihypertensive and anti-fibrotic effects. It can be used to reduce collagen levels in tumor models and can thereby promote the tumor penetration of NPs.[25–28]

In this study, a core-shell structural lipid-polymer hybrid NPs, M/LST-Lip/PTX-PEG$_{5\%}$ was designed which comprised of ROS-degradable LST-loaded polymer micelles core and PTX-loaded transformable lipid shell. The transformation mechanism of the lipid shell relies on the theory that without the presence of a supportive core, the lipid shell would undergo shape transformation from sphere to discoid and would also shrink in size based on the high content of 20% DSPE-PEG2000 and 25% cholesterol.[24] As shown in Figure 1, on its exposure to ROS in the TME, the micelle-core would break down releasing the loaded LST. The released LST would diffuse out of the lipid shell and reduce the levels of collagen in the TME to facilitate further penetration. The smaller discoid lipid NPs can then penetrate deeper into the tumor tissue and deliver the loaded PTX more efficiently. In this study, the NPs were evaluated in terms of their physical properties and in vitro ROS response. The cytotoxicity and the penetrating effect of the NPs on 4T1 tumor spheroids were evaluated and in vivo experiments were also conducted to observe the tumor penetration and inhibition efficacies.

Materials and Methods
Materials
Losartan (LST) and paclitaxel (PTX) were purchased from Sinopharm Chemical Regent Co., LTD (Shanghai, China); PEG-TK-PLA was synthesized by Ruixi Biotechnology Co., LTD (Xi'an, China); 1,2-dioleoyl-3-trimethylammonium-propane
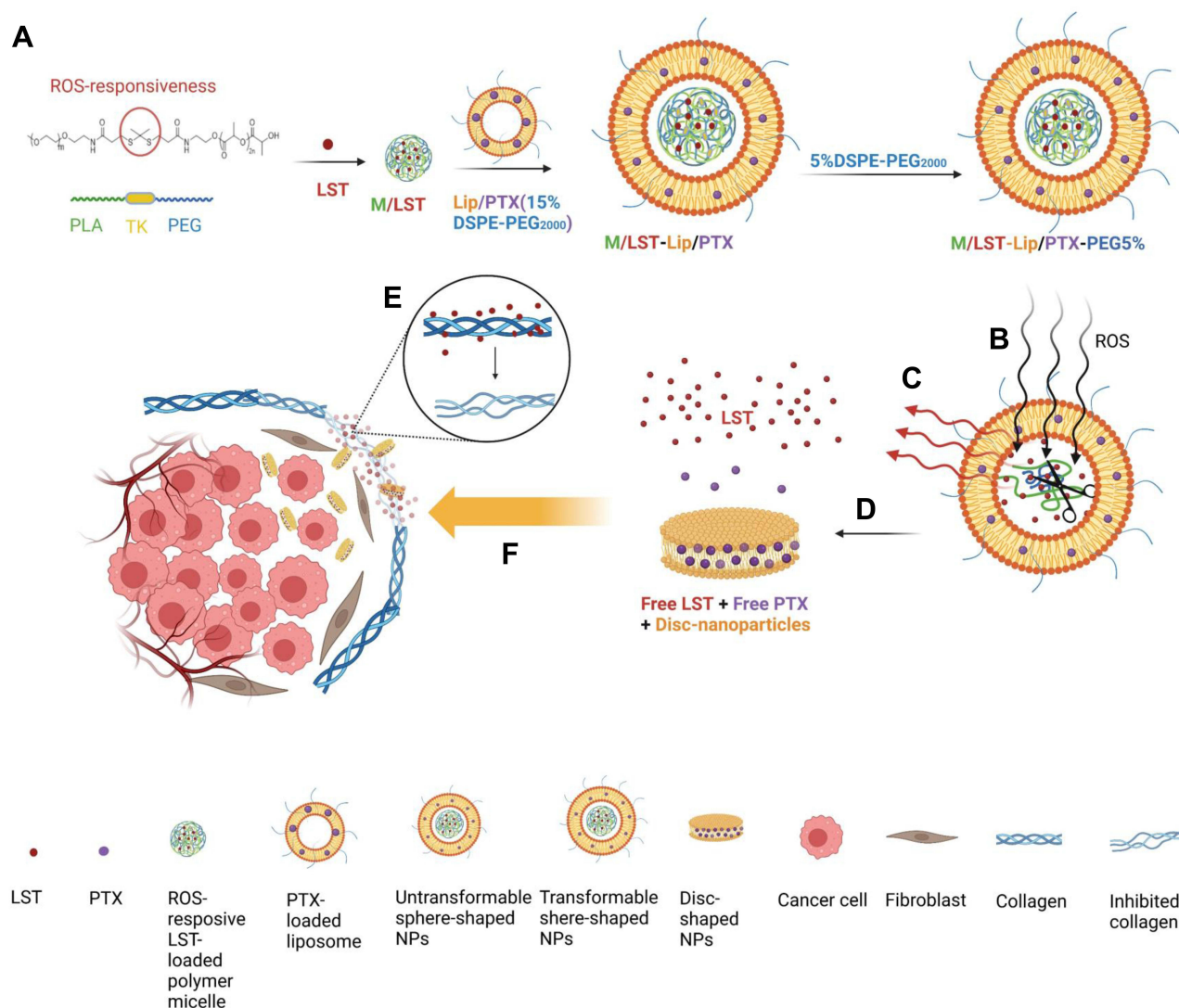
Figure 1 Illustration of preparation and actions of the NPs. (**A**) Preparation of the NPs. (**B**) Reactive oxygen passed through lipid shell, TK bond cleaved and the polymer micelle degraded. (**C**) LST released. (**D**) NPs transformed from spherical to discoid-shape. (**E**) LST acted on collagen in TME. (**F**) Discoid-shaped NPs penetrated into deep tumor and delivered PTX.

Abbreviations: PLA, poly(D, L-lactide); TK, thioketal; PEG, polyethylene glycol; DSPE, 1,2-distearoyl-sn-glycero-3-phosphoethanolamine; NPs, nanoparticles; LST, losartan; PTX, paclitaxel; ROS, reactive oxygen species; M/LST, ROS responsive micelle loaded with LST; Lip/PTX, liposome loaded with PTX; M/LST-Lip/PTX, un-transformable NPs with M/LST as the core and Lip/PTX as the shell; M/LST-Lip/PTX-PEG$_{5\%}$, transformable NPs with M/LST as the core and Lip/PTX as the shell.

(DOTAP) was purchased from Corden Pharma (Switzerland LLC); Hydrogen peroxide was purchased from Nanjing Chemical Reagent Co., LTD (Nanjing, China); D-α-tocopherol polyethylene glycol succinate (TPGS) was purchased from Aladdin Biochemical Technology Co., LTD (Shanghai, China); 1,2-distearoyl-sn-glycero-3-phosphoethanolamine-N-[methoxy(polyethylene glycol)-2000] (DSPE-PEG2000) was purchased from Shanghai AVT Pharmaceutical Technology Co., LTD (Shanghai, China); 1,2-dipalmitoyl-sn-glycero-3-phosphocholine (DPPC) was purchased from Lipoid GmbH (Germany); Cholesterol and Dulbecco's Modified Eagle's Medium (DMEM) were purchased from Sigma Aldrich (USA).

The murine breast cancer 4T1 cell line and fibroblast cell line NIH3T3 were obtained from Chinese Academy of Sciences Cells Bank (Shanghai, China); Coumarin (C6) was purchased from Aladdin Biochemical Technology Co., Ltd (Shanghai, China); Fluorescent dye 1,1′-dioctadecyl-3, 3, 3′, 3′- tetramethyl indotricarbocyanine Iodide (DiR) was purchased from Jiangsu KeyGEN BioTECH Co., Ltd (Nanjing, China); Rhodamine was purchased from Ponsure Biological Co., Ltd (Shanghai, China).

Synthesis of ROS-Responsive Polymer (PLA-TK-PEG)

In brief, 1.0g thioketal (TK) bond-contained polymer mPEG-TK-NH$_2$ and 0.5g lactide were dissolved in 10 mL anhydrous toluene with stannous octoate as catalyst, and the reaction was maintained at 130 °C for 12 h. The mixture solution was concentrated and added to glacial ether. After filtration, precipitation and drying, the PLA-TK-PEG was obtained.

Preparation of ROS-Responsive Micelles

As the core of the hybrid NPs, LST-loaded polymer micelles (M/LST) were prepared by thin film dispersive water method. PLA-TK-PEG (10.0mg, 3.34μMol) and DOTAP (2.0mg, 2.86μMol) were dissolved in 1mL chloroform and LST (0.5mg, 1.14μMol) was dissolved in 1mL methanol, and these solutions were then added into a round-bottom flask. The organic solvent was removed by rotary evaporation for 30min at 55°C and 100rpm, and 2mL reverse osmosis (RO) water was added for rotary hydration at 55°C for 10min. The hydration products were dispersed evenly by transient ultrasound, and the clarified solution of polymer micelles were obtained through 0.22μm filter membrane, namely M/LST.

Preparation of PTX-Loaded Liposomes

PTX-loaded liposomes (Lip/PTX) were prepared by thin film dispersion method. Briefly, 8.6mg DPPC, 8.95mg DSPE-PEG2000, 2.47mg cholesterol (the mole ratio of DSPE-PEG2000:DPPC:Cholesterol was 15:55:30 and the content of DSPE-PEG2000 was 15%) and PTX (0.5mg) were dissolved in 2mL of chloroform at 45°C. Evaporation in vacuum state removed the chloroform to form a film, which was continued to be evaporated for 1h after the solution dried. At 45°C, 2mL RO water was used to hydrate the film for 30min, and the PTX liposome was extruded through 200nm polycarbonate membrane for three times by liposome extruder (Avestin, Canada).

Preparation of Intermediate Hybrid NPs (M/LST-Lip/PTX)

M/LST encapsulated NPs (M/LST-Lip/PTX) were prepared by incubating TPGS aqueous solution, M/LST and Lip/PTX by volume ratio of 1:1:1 at 45°C for 1h, then the final mass concentration of TPGS was 0.05%.

Preparation of the Transformable Hybrid NPs (M/LST-Lip/PTX-PEG$_{5\%}$)

The proportion of DSPE-PEG2000 in lipid shell was increased from 15% to 20% via DSPE-PEG2000 aqueous solution and M/LST-Lip/PTX incubated at 45°C for 1h, and M/LST-LIP/PTX-PEG$_{5\%}$ was obtained.

Preparation of Un-Transformable PEG$_{5\%}$-M/LST-Lip/PTX

We also prepared PEG$_{5\%}$-M/LST-Lip/PTX to illustrate that the encapsulation of M/LST could be disabled if the structure of lipid vesicle was discoid at first, in which the total 20% DSPE-PEG2000 was introduced before hydration of thin film during the preparation of Lip/PTX.

Characterization of the NPs

The average particle size, polydispersity index (PDI) and Zeta potentials of M/LST, Lip/PTX, M/LST-Lip/PTX, M/LST-Lip/PTX-PEG$_{5\%}$ and PEG$_{5\%}$-M/LST-Lip/PTX were measured by dynamic light scattering (DLS, Brookhaven Instruments, NY, USA) at 25°C.

The morphology of M/LST, Lip/PTX, M/LST-Lip/PTX, M/LST-Lip/PTX-PEG$_{5\%}$ and PEG$_{5\%}$-M/LST-Lip/PTX was imaged by transmission electron microscopy (TEM) (HITSCHI, Japan).[29] Images were obtained after 10μL of sample placed over a copper-mesh grid followed by staining with phosphotungstic acid for 3min.

The drug encapsulation efficiency (EE) of M/LST, Lip/PTX and M/LST-Lip/PTX was measured by dialysis, microcolumn centrifugation and ultracentrifugation methods respectively and calculated using Equation 1 and 2.

$$EE\ (LST,\%) = \frac{amount\ of\ LST\ in\ micelles\ or\ NPs}{amount\ of\ total\ LST} \times 100\% \tag{1}$$

$$EE\ (PTX, \%) = \frac{amount\ of\ PTX\ in\ liposomes\ or\ NPs}{amount\ of\ total\ PTX} \times 100\% \qquad (2)$$

In vitro Evaluation of ROS-Responsiveness

The changes in particle size and morphology of M/LST and M/LST-Lip/PTX-PEG$_{5\%}$ under the stimulation of H$_2$O$_2$ were determined by DLS and TEM respectively. The samples were co-cultured with 200μM H$_2$O$_2$ for a certain time and untreated samples (without H$_2$O$_2$) were used as control groups.

In vitro Cytotoxicity on 4T1 cells

The cytotoxicity of blank NPs against 4T1 cells was investigated by methyl thiazolyl tetrazolium (MTT) assay.[30,31] Logarithmic stage 4T1 cells were collected and inoculated in a 96-well plate with 5000 cells/well, incubated at 37°C in a 5% CO$_2$ atmosphere for 24h until cells adhered to the wall. The cells were then treated with different concentrations (100, 200, 500 and 1000μg/mL) of blank NPs (M, M-Lip, M-Lip-PEG$_{5\%}$ and M-Lip-PEG$_{5\%}$-H$_2$O$_2$) for 24h and the negative control group and blank group were set at the same time. Afterwards, the blank NPs solution was removed, 200μL of MTT (0.5mg/mL) solution was added to each well and continued to incubate for 4h. The liquid in the well was then discarded, and150μL of DMSO was added to each well with shaking for 10 min to fully dissolve the crystals. The absorbance at 570 nm of each well was measured with a microplate reader (ELX800, Thermo Fisher, USA), and the cell viability was calculated according to Equation 3.

$$\text{Cell viability}(\%) = \frac{\text{OD}_{\text{sample}} - \text{OD}_{\text{blank}}}{\text{OD}_{\text{control}} - \text{OD}_{\text{blank}}} \qquad (3)$$

OD$_{\text{sample}}$: Absorbance at 570 nm in the administration group.
OD$_{\text{blank}}$: Absorbance at 570 nm in blank group.
OD$_{\text{control}}$: Absorbance at 570 nm in the control group.

In vitro Cytotoxicity on 3D Mixed Tumor Spheroids.

The cytotoxicity of different PTX-loaded NPs against 3D mixed tumor spheroids was completed by MTT assay. The complex tumor spheroids of 4T1 and activated fibroblast cell line NIH3T3 were co-cultured together by hanging drop method.[17,32,33] The activated NIH3T3 and 4T1 were digested with 0.25% trypsin and collected, which were diluted with 0.24% methylcellulose solution and adjusted to a concentration of 8×10^4/mL. 4T1 and NIH3T3 were mixed in a 3:1 ratio. After 7-day cultivation, mixed tumor spheroids were incubated with PTX/LST solution, M-Lip/PTX-PEG$_{5\%}$, M/LST-Lip /PTX and M/LST-Lip/PTX-PEG$_{5\%}$ for 48 h with the final concentrations of PTX set at 5, 25, 50, 75 and 100 μg/mL in DMEM medium, respectively. Afterwards, the drug solution was removed, 200μL of MTT (0.5mg/mL) solution was added to each well and continued to incubate for 4h. The liquid in the well was then discarded, 150μL of DMSO was added to each well with shaking for 10 min to fully dissolve the crystals. The absorbance at 570 nm of each well was measured with a microplate reader (ELX800, Thermo Fisher, USA), and the cell viability was calculated according to Equation 3.

In vitro Penetration in 3D Tumor Spheroids

The coumarin (C6) was used as fluorescent substance, and Lip/C6, M/LST-Lip/C6, M-Lip/C6 and M/LST-Lip/C6-PEG$_{5\%}$ were prepared as described methods in the previous sections.

A 3D tumor spheroid model was used to verify the penetration ability of the NPs in vitro.[12,34–36] Logarithmic stage 4T1 cells were collected and diluted into cell suspension of 8×10^4 cell/mL in a complete culture medium containing 0.24% methyl cellulose. 25μL/drop suspensions were deposited onto a lid of a cell culture dish. PBS was added into the dish and the lid was then inverted and covered the dish base. After incubation at 37°C with 5% CO$_2$ for 24h, the cell masses were transferred to a 96-well plate coated with 1.5% agarose and continued to be cultured to an appropriate size, during which the fluid was changed every two and a half days. The tumor spheroids with uniform size and compact shape were selected and treated with the same amount of free C6, Lip/C6, M-Lip/C6, M/LST-Lip/C6 and M/LST-Lip/C6-PEG$_{5\%}$. After cultured at 37°C with 5% CO$_2$ for 12h, the culture medium was carefully removed, and the tumor

spheroids were carefully cleaned with pre-cooled PBS for 3 times, fixed with 4% paraformaldehyde for 30min, and rinsed with PBS for 3 times. The tumor spheroids were moved to a confocal dish, and Z-stack tomography was performed with confocal laser scanning microscope (CLSM, LSM800, Zeiss, Germany) and photographs were taken.

In vitro Penetration Capacity in 3D Mixed Tumor Spheroids

To investigate the promoting effect of LST on penetration, the complex tumor spheroids of 4T1 and activated fibroblast cell line NIH3T3 were co-cultured together as described in the previous section of cytotoxicity. The subsequent processes were the same as the previous section of penetration in 3D tumor spheroids. The radius R of the tumor sphere was measured from the bright field image. The fluorescent circle with the largest radius was selected as the cross section with the deepest penetration distance, and the radius of this cross section was measured as r. The penetration efficiency (%) of different C6 NPs in the 3D mixed tumor spheroids was calculated as r/R, and higher penetration efficiency indicates deeper penetration distance.

Tumor-Bearing Mice Model

4T1 cells at logarithmic growth stage were prepared into cell suspensions of 1×10^7/mL with PBS under aseptic conditions, and the tumor-bearing mice model of in situ breast cancer was established by 0.1 mL subcutaneously inoculated into the fourth pair of left mammary fat pads of Balb/C mice.

All animal experiments were approved by Institutional Animal Care Committee of the China Pharmaceutical University, and all animal studies were performed in compliance with the guidelines of the committee. The ethical code was No.20200828–001.

In vivo Tumor-Targeting Efficacy

DiR was used as fluorescent substance, Lip/DiR, M/LST-Lip/DiR, M-Lip/DiR and M/ LST-Lip/DiR-PEG$_{5\%}$ were prepared as described methods in the previous sections.

When the tumor volume reached 100–200 mm^3, the tumor-bearing mice were randomly divided into 4 groups with 3 mice in each group. Free DiR and DiR loaded NPs were injected into tail vein at the dose of 1mg/kg DiR. Whole-body imaging was performed at 2, 4, 8 and 12 h of post-injection. At 12 h of post-injection, the major organs (heart, liver, spleen, lung and kidney) and tumor were excised and photographed on an in vivo imaging system (PerkinElmer Ivis Spectrum) with appropriated wavelengths (excitation/emission, 750/780nm).

In vivo Antitumor Efficacy

When the tumor volume reached 150–200mm^3, the tumor-bearing mice were randomly divided into 6 groups with 5 mice in each group. Normal saline, free LST+PTX, M/LST, M/LST-Lip/PTX-PEG$_{5\%}$ and M/LST-Lip/PTX-PEG$_{5\%}$ were iv injected respectively at the dose of 10mg/kg. Tumor volume was recorded at 0, 2, 4, 6, 8 and 10 days to evaluate the tumor inhibition of the therapeutic efficacy of the treatments.

Table 1 Average Particle Size, PDI and Zeta Potential of the NPs

NPs	Size (nm)	PDI	Zeta Potential (mV)	EE% (LST)	EE% (PTX)
M/LST	117.78±0.72	0.264±0.011	35.30±3.33	67.58%	–
Lip/PTX	109.80±4.08	0.287±0.011	–	–	32.7%
M/LST-Lip/PTX	129.08±7.45	0.207±0.021	−7.22±1.20	46.28%	14.12%
M/LST-Lip/PTX-PEG$_{5\%}$	143.51±3.76	0.273±0.024	–	–	–
PEG$_{5\%}$-M/LST-Lip/PTX	125.35±3.44	0.269±0.002	–	–	–

Note: The results are expressed as the mean ± SD, n=3.
Abbreviations: LST, losartan; PTX, paclitaxel; PDI, polydispersity index; EE, encapsulation efficiency; M/LST, reactive oxygen species (ROS) responsive micelles loaded with LST; Lip/PTX, liposomes loaded with PTX; M/LST-Lip/PTX, un-transformable hybrid NPs with M/LST as the core and Lip/PTX as the shell; M/LST-Lip/PTX-PEG$_{5\%}$, transformable hybrid NPs with modified lipid shell; PEG$_{5\%}$-M/LST-Lip/PTX, un-transformable hybrid NPs with 20% DSPE-PEG2000 introduced in Lip/PTX.
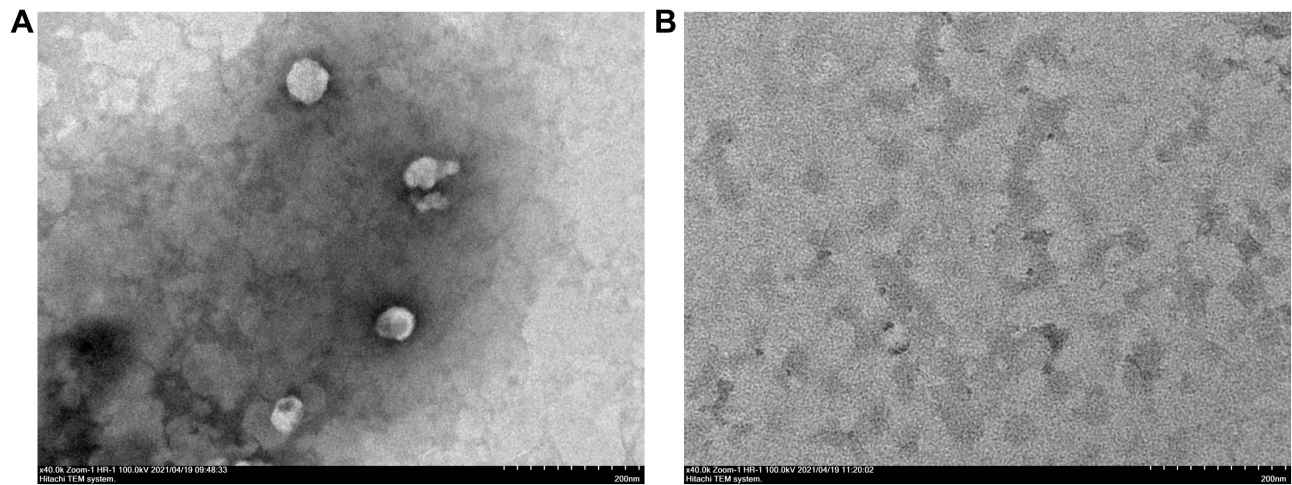
Figure 2 TEM images of M/LST without (**A**) and with (**B**) H_2O_2.
Abbreviations: M/LST, reactive oxygen species (ROS) responsive micelles loaded with losartan; TEM, transmission electron microscopy.
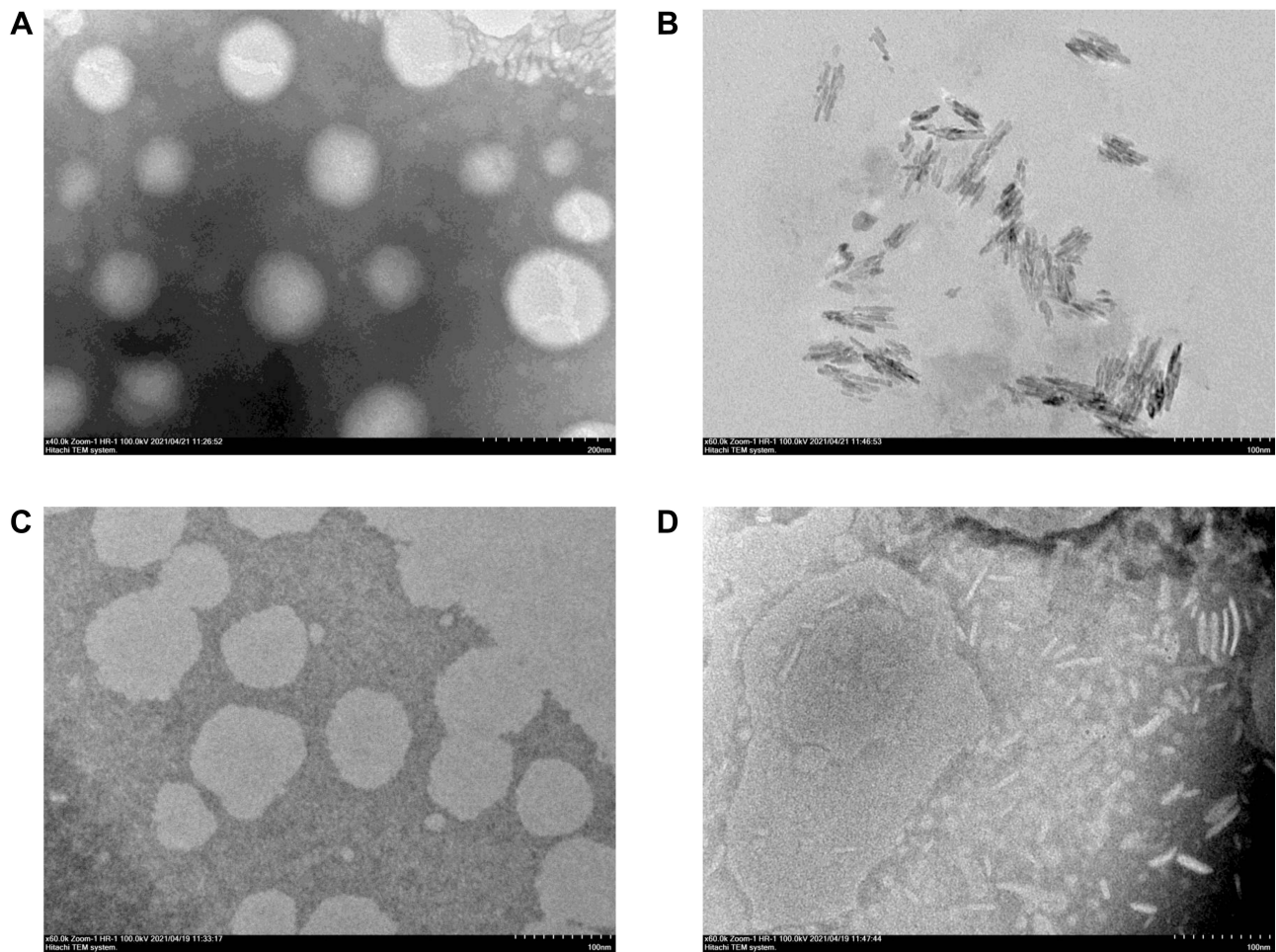

Figure 3 TEM images of (**A**) M/LST-Lip/PTX, (**B**) PEG$_{5\%}$-M/LST-Lip/PTX, (**C**) M/LST-Lip/PTX-PEG$_{5\%}$, and (**D**) M/LST-Lip/PTX-PEG$_{5\%}$ after adding H_2O_2.
Abbreviations: TEM, transmission electron microscopy; LST, losartan; PTX, paclitaxel; M/LST, reactive oxygen species (ROS) responsive micelles loaded with LST; Lip/PTX, liposomes loaded with PTX; M/LST-Lip/PTX, un-transformable hybrid NPs with M/LST as the core and Lip/PTX as the shell; M/LST-Lip/PTX-PEG$_{5\%}$, transformable hybrid NPs with modified lipid shell; PEG$_{5\%}$-M/LST-Lip/PTX, un-transformable hybrid NPs with 20% DSPE-PEG2000 in Lip/PTX.

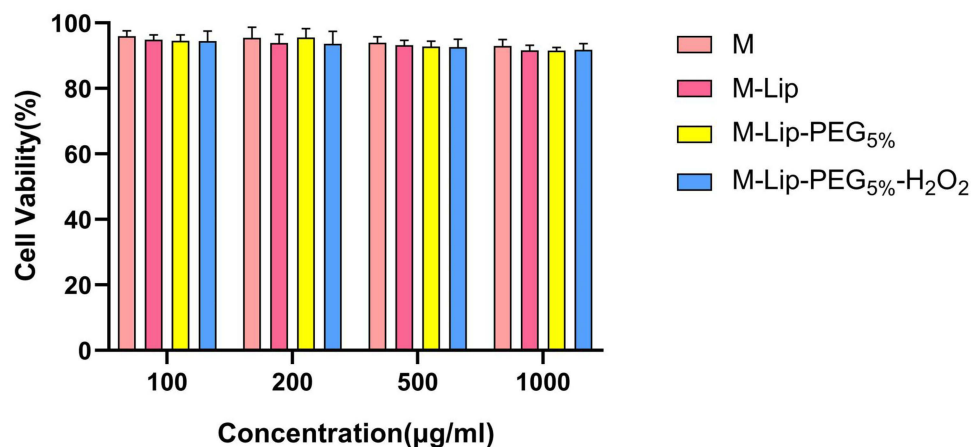**Figure 4** Cell viability of 4T1 cells incubated with blank NPs.
Note: The results are expressed as the mean ± SD, n=3.
Abbreviations: M, reactive oxygen species (ROS) responsive micelles; M-Lip, blank un-transformable hybrid NPs; M-Lip-PEG$_{5\%}$, blank transformable hybrid NPs; M-Lip-PEG$_{5\%}$-H$_2$O$_2$, blank transformable hybrid NPs treated with H$_2$O$_2$.

In vivo Tumor-Penetrating Efficiency

Rhodamine was used as fluorescent substance. Lip/Rhodamine, M/LST-Lip/Rhodamine, M-Lip/Rhodamine and M/LST-Lip/Rhodamine-PEG$_{5\%}$ were prepared as described methods in the previous sections.

When the tumor volume reached 100–200mm^3, the mice were iv injected with free Rhodamine or Rhodamine loaded NPs respectively at the dose of 1mg/kg (5 mice in each group). At 24h of post-injection, fresh tumors were excised for embedding, fixation and sectioning (thickness about 4mm) with OCT frozen embedding agent. Immunofluorescence assay of tumor tissue vascular marker protein CD31 was performed. Anti-CD31 staining was performed at 4°C overnight, and then anti-Alex488 staining was performed for 1 hour and DAPI dying for 10 minutes. Images were taken by CLSM.
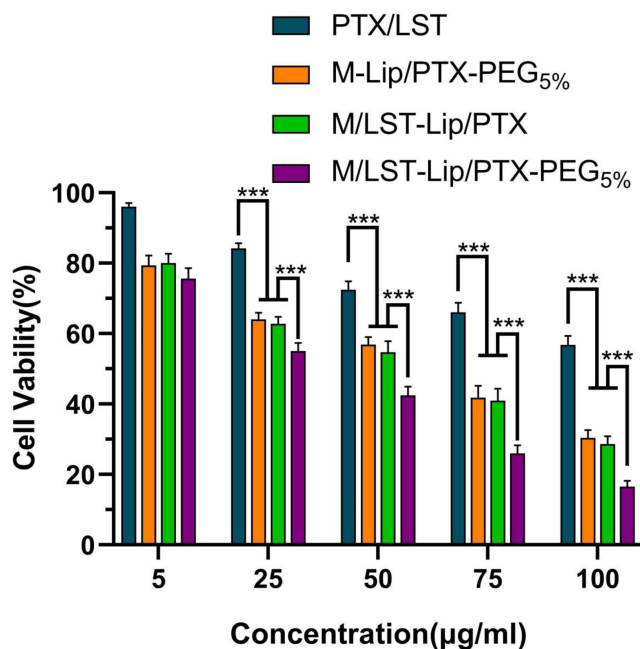

Figure 5 Cell viability of 4T1 cells in 3D mixed tumor spheroid incubated with PTX-loaded NPs.
Note: The results are expressed as the mean ± SD, n=3, ***p < 0.001.
Abbreviations: LST, losartan; PTX, paclitaxel; M/LST, reactive oxygen species (ROS) responsive micelles loaded with LST; Lip/PTX, liposomes loaded with PTX; M, reactive oxygen species (ROS) responsive micelles; M-Lip/PTX, un-transformable hybrid NPs with M as the core and Lip/PTX as the shell; M/LST-Lip/PTX, un-transformable hybrid NPs with M/LST as the core and Lip/PTX as the shell; M/LST-Lip/PTX-PEG$_{5\%}$, transformable hybrid NPs with M/LST as the core and Lip/PTX as the shell.
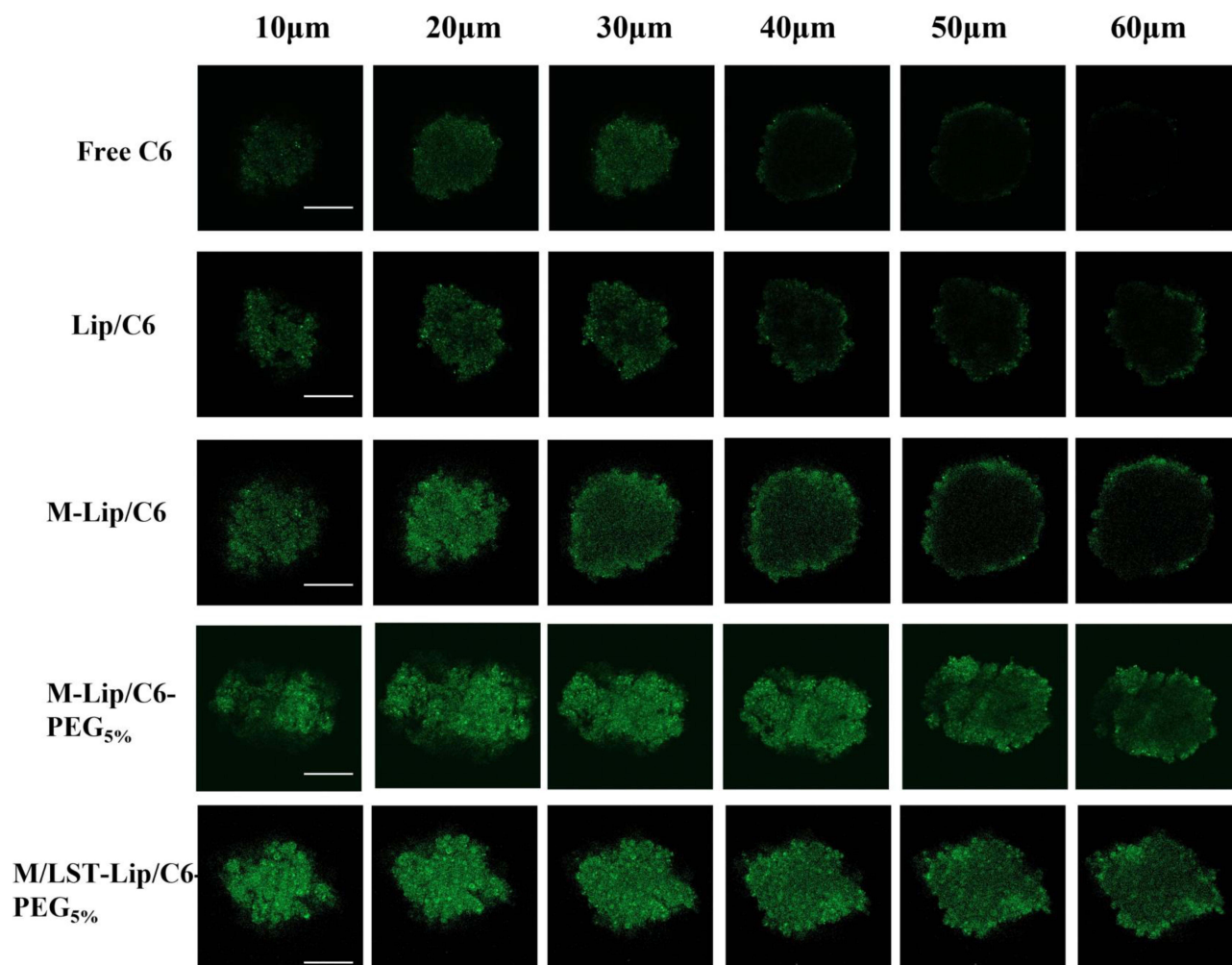
Figure 6 CLSM images of 4T1 tumor sphere incubated with C6-loaded NPs, scale =100nm.
Abbreviations: CLSM, confocal laser scanning microscope; C6, coumarin 6; Lip/C6, liposomes loaded with C6; M-Lip/C6, un-transformable hybrid NPs loaded with C6 on the lipid shell; M-Lip/C6-PEG$_{5\%}$, transformable hybrid NPs loaded with C6 on the lipid shell; M/LST-Lip/C6-PEG$_{5\%}$, transformable hybrid NPs loaded with losartan in the micelle core and C6 on the lipid shell.

Statistical Analysis

All the experiments were conducted at least three times and all data were presented as mean ± standard deviation (SD). Obtained results were analyzed by ANOVA.[37] Statistical significance was showed as ****$p<0.0001$, ***$p<0.001$, **$p<0.01$ and *$p<0.5$.

Results and Discussion

Preparation of the NPs

Discoid lipid NPs can be obtained by using specific compositions of DSPE-PEG2000 and cholesterol.[24] In this study, the DSPE-PEG2000 and cholesterol content was kept at 20% and 25% respectively. As discoid-structured lipid NPs are incapable of encapsulating micelle-cores to form hybrid NPs, spherical liposomes (Lip/PTX) were first prepared with 15% DSPE-PEG2000. After encapsulation of the ROS-responsive micelle cores, the intermediate hybrid NPs (M/LST-Lip/PTX) was modified by increasing the content of DSPE-PEG2000 from 15% to 20%. And finally, the transformable lipid-polymer hybrid NPs (M/LST-Lip/PTX-PEG$_{5\%}$) were obtained.

Characterization of M/LST, Lip/PTX, M/LST-Lip/PTX, and M/LST-Lip/PTX-PEG$_{5\%}$

The average particle size, polydispersity index (PDI), and Zeta potentials of M/LST, Lip/PTX, M/LST-Lip /PTX, and M/LST-Lip/PTX-PEG$_{5\%}$ have been depicted in Table 1. After introducing the micelles (M/LST) into the liposomes, the Zeta potential of M/LST-Lip/PTX was −7.22±1.20 mV, and the flipping of charge confirmed the assembly of M/LST into Lip/PTX.

The EE% of M/LST, Lip/PTX, and M/LST-Lip/PTX has been listed in Table 1. The EE% of LST in M/LST was 67.58%, indicating the proper encapsulation of LST in the micelles. Due to the simultaneous release of LST in M/LST during dialysis, the measured efficacy was low. In other words, the EE% of LST in M/LST might be higher.

Evaluation of in-vitro ROS Responsiveness

Figure 2A shows the microstructure of M/LST. The M/LST had a particle size of about 40 nm with evenly distributed spherical morphology. The smaller particle size may be attributed to the fact that TEM reflects the sample size in the dry state, while the size measured by the laser scattering method was that of the hydrodynamic diameter in a hydrated state. NPs have been reported to show larger hydrodynamic volumes in the hydrated state due to solvent effects.[38] TEM images of M/LST after the addition of H_2O_2 have been shown in Figure 2B, which reflects the complete degradation of M/LST after 8h of the addition of H_2O_2, and the absence of micellar structure indicates the ROS responsiveness of M/LST.

Figure 3A shows the microstructure of M/LST-Lip/PTX which is a uniform and solid spherical structure with a particle size of about 120 nm that is consistent with the data in Table 1. Figure 3B shows the microstructure of discoid-shaped PEG$_{5\%}$-M/LST-Lip/PTX. The discoid-shaped structure is due to the presence of 20% DSPE-PEG2000 in PEG$_{5\%}$-M/LST-Lip/PTX, which was introduced during the preparation of Lip/PTX. Figure 3C shows the spherical microstructure of M/LST-Lip/PTX-PEG$_{5\%}$, with a particle size of about 130nm which is consistent with the data presented in Table 1. The M/LST-Lip/PTX-PEG$_{5\%}$ shown in Figure 3C also contains 20% DSPE-PEG2000, out of which, 15% was introduced during Lip/PTX preparation and another 5% was introduced post-incubation. Figure 3D shows the discoid microstructure of M/LST-Lip/PTX-PEG$_{5\%}$ after exposure to H_2O_2 for 8h. This was consistent with the expectation that under the stimulation of H_2O_2, the polymer micelle degrades, and the outer shell shrinks to a smaller size and eventually transforms from a spherical-shaped structure to
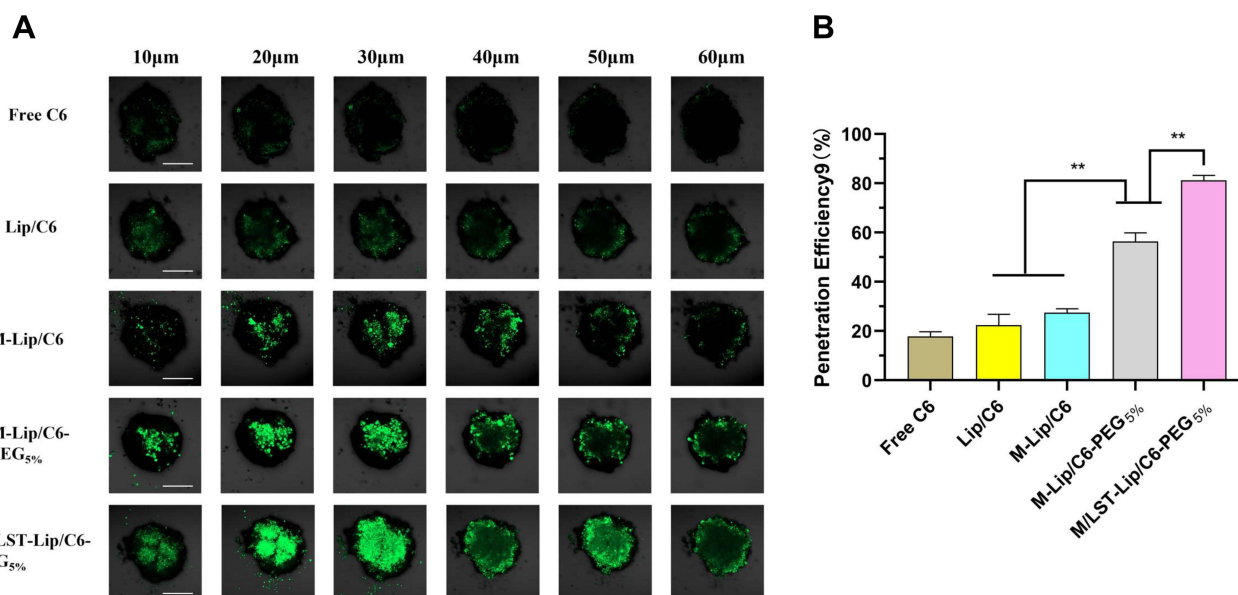

Figure 7 (**A**) CLSM images and (**B**) fluorescence penetration efficiency in 4T1 tumor spheroids incubated with NPs loaded with C6, scale =100 nm.
Note: The results are expressed as mean ± SD, n=3, **p < 0.01.
Abbreviations: CLSM, confocal laser scanning microscope; C6, coumarin 6; Lip/C6, liposomes loaded with C6; M-Lip/C6, un-transformable hybrid NPs loaded with C6 on the lipid shell; M-Lip/C6-PEG$_{5\%}$, transformable hybrid NPs loaded with C6 on the lipid shell; M/LST-Lip/C6-PEG$_{5\%}$, transformable hybrid NPs loaded with losartan in the micelle core and C6 on the lipid shell.

a discoid-shaped structure. These findings are in agreement with the results of other investigations reporting the sulfhydryl-mediated degradation of thioketal conjugated NPs upon the stimuli of H_2O_2.[39,40]

In vitro Cytotoxicity on 4T1 Cells

Blank NPs without LST and PTX were studied to evaluate their cytotoxicity against 4T1 cells. Cells were developed using the traditional 2D cell culture technique. As shown in Figure 4, the cell survival rates were above 90% at all test concentrations, and no significant difference between different blank NPs was observed, indicating the nanocarriers exhibited nontoxicity at test concentrations.

In vitro Cytotoxicity on 3D Mixed Tumor Spheroids

The toxicity of M-Lip/PTX-PEG$_{5\%}$, M/LST-Lip/PTX, and M/LST-Lip/PTX-PEG$_{5\%}$ to 3D mixed tumor spheroids was higher than that of free drug PTX/LST (Figure 5). The increased cytotoxicity of M-Lip/PTX-PEG$_{5\%}$ may be related to the enhanced penetration of micelles into tumor spheres. The increase in cytotoxicity may be related to the decrease in collagen content in tumor spheres by LST. When the concentration of PTX was 100μg/mL, the inhibition rates of M/LST-Lip/PTX-PEG$_{5\%}$ were 1.17 times and 1.20 times than those of M/LST-Lip/PTX and M-Lip /PTX-PEG$_{5\%}$, respectively, indicating that the dual strategy could significantly inhibit the growth of 3D mixed tumor spheroids at the in vitro level.
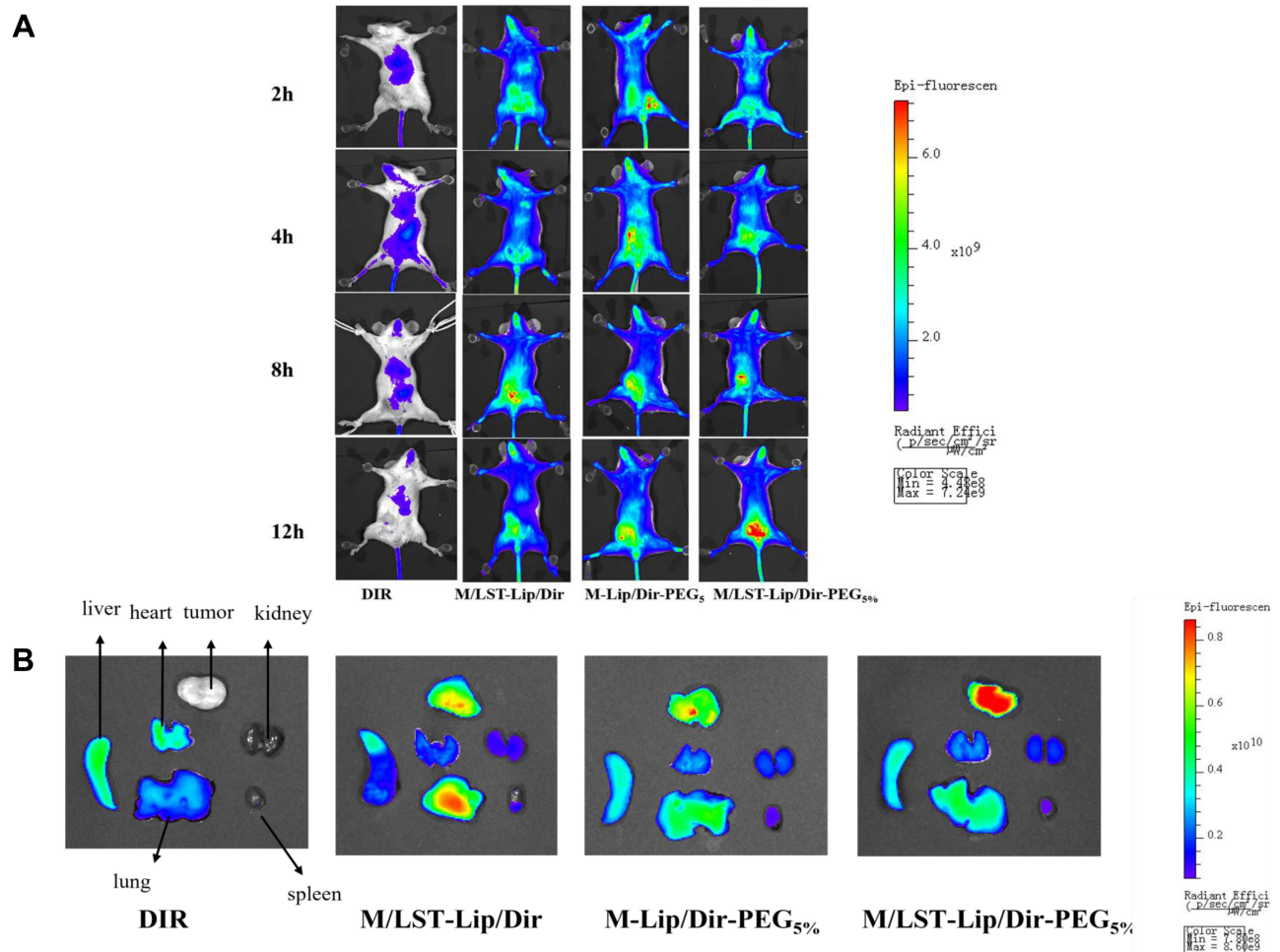

Figure 8 (**A**) In vivo imaging of tumor-bearing mice after administration of DiR, M/LST-Lip/DiR, M-Lip/DiR-PEG$_{5\%}$ and M/LST-Lip/DiR-PEG$_{5\%}$; (**B**) Ex vivo images of tissues including heart, liver, spleen, lung, kidney, and tumor collected at 12 h post-injection of DiR, M/LST-Lip/DiR, M-Lip/DiR-PEG$_{5\%}$ and M/LST-Lip/DiR-PEG$_{5\%}$.
Abbreviations: DiR, Fluorescent dye DiR; LST, losartan; M/LST-Lip/DiR, un-transformable hybrid NPs loaded with LST in the micelle-core and DiR on the lipid shell; M-Lip/DiR-PEG$_{5\%}$, transformable hybrid NPs loaded with DiR on the lipid shell; M/LST-Lip/DiR-PEG$_{5\%}$, transformable hybrid NPs loaded with LST in the micelle-core and DiR on the lipid shell.

In vitro Penetration Capacity in 3D Tumor Spheroids

NPs loaded with C6 were prepared and their in vitro penetrations in 4T1 tumor spheroids were studied using Z-stack at 10-μm intervals from apex to the equator. Figure 6 shows the scanning and photographing results. Free C6 was difficult to penetrate deep into the tumor, and also the fluorescence signal was weak and uneven. Lip/C6 and M-Lip/C6 showed strong fluorescence signals on the periphery of tumor spheroids but not in the interior. In contrast, M-Lip/C6-PEG$_{5\%}$ and M/LST-Lip/C6-PEG$_{5\%}$ could penetrate throughout the spheroids and deliver C6 to the interior regions. This suggests the success of the size/shape adjustable strategy in enhancing the penetration ability of the NPs. However, no significant difference between the fluorescence signal of NPs with and without LST was observed, indicating that LST played no role in this tumor spheroid model which consisted of onefold 4T1 cells.

In vitro Penetration Capacity in 3D Mixed Tumor Spheroids

The fibroblasts in the mixed tumor spheroids secreted collagen to simulate the in vivo physiological conditions. The penetration of NPs without LST (Lip/C6, M-Lip/C6, and M-Lip/C6-PEG$_{5\%}$) was inhibited by collagens in contrast to that of M/LST-Lip/C6-PEG$_{5\%}$ (Figure 7). This can explain the inability of LST to improve the penetration of correspondent NPs in 4T1 tumor spheroids. However, in mixed tumor spheroids, the introduction of LST increased the penetration efficacy of M/LST-Lip/C6-PEG$_{5\%}$ by 1.44 times compared to that of M-Lip/C6-PEG$_{5\%}$. Alternatively, the penetration of M-Lip/C6-PEG$_{5\%}$ was also significantly higher than that of M-Lip/C6. The results indicated that the deep penetration of NPs in mixed tumor spheroids was achieved through the synergistic effect of LST and discoid morphology, which was launched by ROS-triggered release and transformation.

In vivo Tumor-Targeting Efficacy

The tumor-targeting effect of the NPs was examined in 4T1 tumor-bearing mice after intravenous (IV) injection and DiR fluorescence (λex/em: 750/780nm) was used for imaging. The accumulation of M/LST-Lip/DiR, M-Lip/DiR-PEG$_{5\%}$, and M/
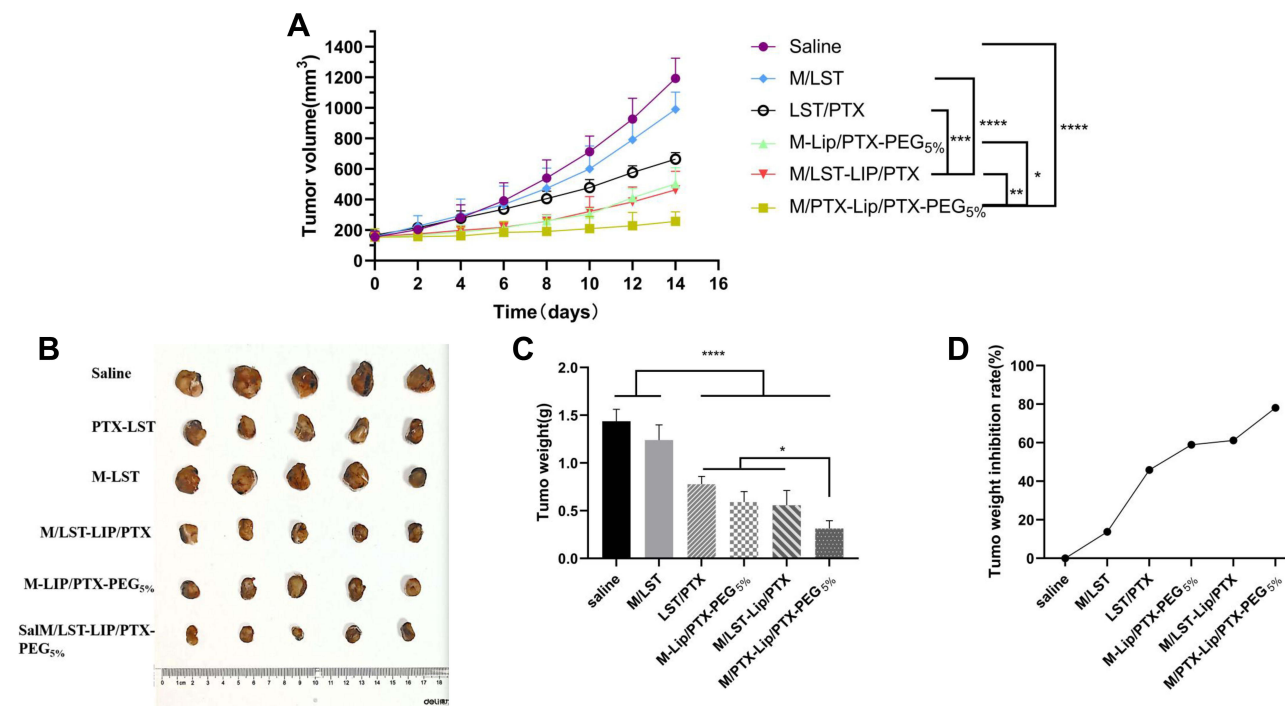

Figure 9 In vivo antitumor effect of normal saline, LST+PTX, M/LST-Lip/PTX, M-Lip/PTX-PEG$_{5\%}$ and M/LST-Lip/PTX-PEG$_{5\%}$ in tumor-bearing mice model. (**A**) Changes in tumor volume, (**B**) Digital images of tumor tissue collected on day 14, (**C**) and (**D**) tumor weight and tumor growth inhibition rate.
Notes: The results are expressed as mean ± SD, n=5; *p < 0.5, **p < 0.01, ****p < 0.0001.
Abbreviations: LST, losartan; PTX, paclitaxel; M/LST, reactive oxygen species (ROS) responsive micelles loaded with LST; Lip/PTX, liposomes loaded with PTX; M/LST-Lip /PTX, un-transformable hybrid NPs with M/LST as the core and Lip/PTX as the shell; M/LST-Lip/PTX-PEG$_{5\%}$, transformable hybrid NPs.

LST-Lip/DiR-PEG$_{5\%}$ in tumor sites increased with time post the IV injection, while the accumulation of free DiR was mainly in the liver and not in the tumor sites (Figure 8A). At 12h post-injection, the fluorescence intensity of M-Lip/DiR-PEG$_{5\%}$, and M/LST-Lip/DiR-PEG$_{5\%}$ in the tumor reached their maximum respectively, and M/LST-Lip/DiR-PEG$_{5\%}$ was higher than in other groups. The fluorescence intensity of M/LST-Lip/DiR peaked at 8 h post-injection, turning weak thereafter. In Figure 8B, fluorescence distribution showed that 12h post-injection, M/LST-Lip/DiR, and M-Lip/DiR-PEG$_{5\%}$ also accumulated in the tumor site, but in an amount lesser than M/LST-Lip/DiR-PEG$_{5\%}$, which was consistent with the deep penetration of M/LST-Lip/DiR-PEG$_{5\%}$ in the in vitro 3D mixed tumor spheroids. These results demonstrated that the introduction of LST reduced the production of collagens in the TME, relieved constriction, and promoted the delivery of NPs into the tumors. Moreover, increasing PEG content enabled the transformation of NPs to discoid shape, facilitating deeper tumor penetration, thereby proving that LST and increasing PEG content mutually promoted accumulation at the tumor site.

In vivo Antitumor Efficacy

The in vivo antitumor effect of the NPs on 4T1 tumor-bearing mice was tested. As shown in Figures 9A and B, for mice treated with saline and M-LST, rapid tumor growth was observed, and the tumor volume was 7.7 and 6.3 times respectively compared to the initial after 14 days. For mice treated with free LST+PTX, M/LST-Lip/PTX, M-Lip/PTX-PEG$_{5\%}$, and M/LST-Lip/PTX-PEG$_{5\%}$, tumor growth was inhibited by 45.90%, 61.20%, 58.97%, and 78.16%, respectively. Compared to M/LST and LST/PTX, the groups treated with M/LST-Lip/PTX and M-Lip/PTX-PEG$_{5\%}$ presented a more notable decrease in tumor volume, indicating that a single strategy, ether collagen inhibition or size/shape transformation could increase tumor penetration and then enhance antitumor efficacy. But the inhibition rate of M/LST-Lip/PTX-PEG$_{5\%}$ was 1.28 times and 1.33 times higher than that of the M/LST-Lip/PTX and M-Lip/PTX-PEG$_{5\%}$ respectively (Figure 9C and D), demonstrating that single strategy is suboptimal and utilizing dual strategies could significantly inhibit tumor growth.
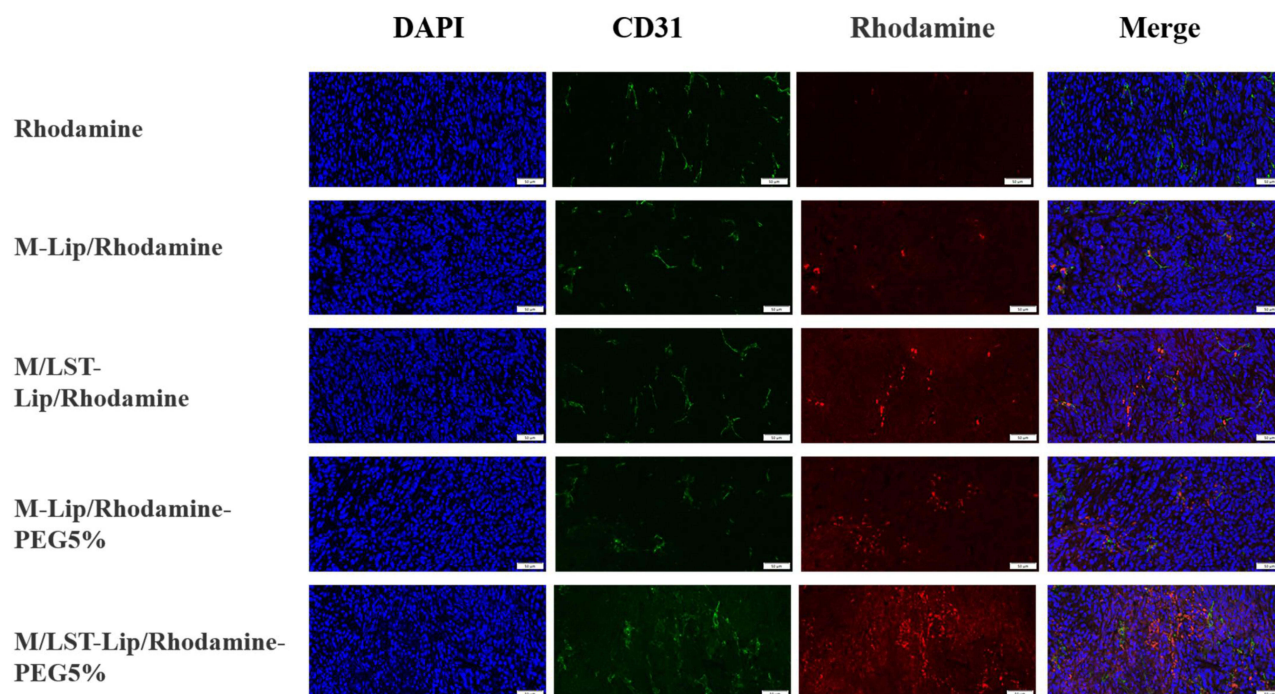

Figure 10 Laser confocal images of tumor tissues after iv injection of free Rhodamine, M-Lip/Rhodamine, M/LST-Lip/Rhodamine, M-Lip/Rhodamine-PEG$_{5\%}$ and M/LST-Lip/Rhodamine-PEG$_{5\%}$ for 12 h (Blue, DAPI-stained nuclei; green, anti-CD31 antibody-labeled tumor vessels; red: Rhodamine-labeled nanocarriers. Scale bars = 50 μm).
Abbreviations: M-Lip/Rhodamine, un-transformable hybrid NPs loaded with Rhodamine on the shell; M/LST-Lip/Rhodamine, un-transformable hybrid NPs loaded with LST in the micelle-core and Rhodamine on the lipid shell; M-Lip/Rhodamine-PEG$_{5\%}$, transformable hybrid NPs loaded with Rhodamine on the lipid shell; M/LST-Lip/Rhodamine-PEG$_{5\%}$, transformable hybrid NPs loaded with LST in the micelle-core and Rhodamine on the lipid shell.

In vivo Tumor-Penetrating Efficiency

To further investigate the tumor penetrating behavior of the NPs in vivo, 4T1 tumor-bearing mice were intravenously injected with free Rhodamine and Rhodamine loaded NPs respectively. After IV injection of free Rhodamine and M-Lip/Rhodamine, there was a lower red fluorescence signal in the tumor, indicating the difficulty of free Rhodamine and un-transformable NPs to enter the tumor tissue (Figure 10). However, for mice treated with M/LST-Lip/Rhodamine and M-Lip/Rhodamine-PEG$_{5\%}$ the fluorescence intensity increased but distributed near the blood vessels, indicating that the two NPs could achieve extravacation, but their accumulation in the tumor was still not obvious. In contrast, the red fluorescence signal of M/LST-Lip/Rhodamine-PEG$_{5\%}$ was the strongest, indicating that LST and transformed discoid NPs jointly promoted the accumulation at tumor sites in mice. It is noteworthy that the in vivo penetrating efficacy of the NPs is related to their penetration effects on in vitro 3D mixed tumor spheroids, and that the transformable hybrid NPs loaded with LST exhibited the optimum efficiency compared to un-transformable and LST-free ones. These findings are consistent with previous studies that have shown the effect of LST on facilitating deeper tumor penetration.[25,27]

Conclusions

In summary, we designed a core-shell structural NPs drug delivery system, M/LST-Lip/PTX-PEG$_{5\%}$, with ROS-responsiveness and size-/shape-transformability for effective tumor accumulation and penetration. M/LST-Lip/PTX-PEG$_{5\%}$ undergoes ROS-triggered core-cleave and LST release to TME, the remained NPs transform from sphere to discoid and penetrate into deep tumors and release loaded PTX. M/LST-Lip/PTX-PEG$_{5\%}$ exhibited potent antitumor efficacy in mouse tumor models. The results of in vitro experiments showed that the NPs could degrade to smaller and discoid carriers in response to reactive oxygen (H_2O_2). In vitro and in vivo investigations of tumor penetration indicate that the NPs could penetrate deep into tumor tissue, owing to LST acting on TME collagen tissue and the dual-transformability on size and shape. In vivo efficacy experiments had proven that M/LST-Lip/PTX-PEG$_{5\%}$ present effective antitumor activity. Our work demonstrates the successful development of a multifunctional NPs with TME-modulated activity and deeply tumor-penetrating effect. This novel drug delivery platform is a promising new candidate for tumor treatment.

Disclosure

The authors report no conflicts of interest in this work.

References

1. Yoo JW, Chambers E, Mitragotri S. Factors that control the circulation time of nanoparticles in blood: challenges, solutions and future prospects. *Curr Pharm Des*. 2010;16(21):2298–2307. doi:10.2174/138161210791920496
2. Hanahan D, Weinberg AR. Hallmarks of cancer: the next generation. *Cell*. 2011;144(5):646–674. doi:10.1016/j.cell.2011.02.013
3. Yamauchi M, Barker HT, Gibbons LD, Kurie MJ. The fibrotic tumor stroma. *J Clin Invest*. 2018;128(1):16–25. doi:10.1172/JCI93554
4. Pickup MW, Mouw JK, Weaver VM. The extracellular matrix modulates the hallmarks of cancer. *EMBO Rep*. 2014;15(12):1243–1253. doi:10.15252/embr.201439246
5. Sakai S, Iwata C, Tanaka YH, et al. Increased fibrosis and impaired intratumoral accumulation of macromolecules in a murine model of pancreatic cancer co-administered with FGF-2. *J Control Release*. 2016;230:109–115.
6. Moghimi MS, Hunter CA, Murray CJ. Long circulating and target-specific nanoparticles: theory to practice. *Pharmacol Rev*. 2001;53(2):283–318.
7. Cabral H, Matsumoto Y, Mizuno K, et al. Accumulation of sub-100 nm polymeric micelles in poorly permeable tumours depends on size. *Nat Nanotechnol*. 2011;6(12):815–823.
8. Dreher RM, Liu WG, Michelich RC, Dewhirst WM, Yuan F, Chilkoti A. Tumor vascular permeability, accumulation, and penetration of macromolecular drug carriers. *J Natl Cancer Inst*. 2006;98(5):335–344.
9. Popović Z, Liu WH, Chauhan PV, et al. A nanoparticle size series for in vivo fluorescence imaging. *Angew Chem Int Ed Engl*. 2010;49(46):8649–8652.
10. Wang JQ, Mao WW, Lock LL, et al. The role of micelle size in tumor accumulation, penetration, and treatment. *ACS Nano*. 2015;9(7):195–206. doi:10.1021/acsnano.5b02017
11. Vlashi E, Kelderhouse EL, Sturgis EJ, Low SP. Effect of folate-targeted nanoparticle size on their rates of penetration into solid tumors. *ACS Nano*. 2013;7(10):8573–8582. doi:10.1021/nn402644g
12. Huang KY, Ma HL, Liu J, et al. Size-dependent localization and penetration of ultrasmall gold nanoparticles in cancer cells, multicellular spheroids, and tumors in vivo. *ACS Nano*. 2012;6(5):4483–4493. doi:10.1021/nn301282m
13. Sonavane G, Tomoda K, Makino K. Biodistribution of colloidal gold nanoparticles after intravenous administration: effect of particle size. *Colloids Surf B Biointerfaces*. 2008;66(2):274–280. doi:10.1016/j.colsurfb.2008.07.004

14. Park J, Maltzahn G, Zhang LL, et al. Systematic surface engineering of magnetic nanoworms for in vivo tumor targeting. *Small*. 2009;5 (6):694–700. doi:10.1002/smll.200801789

15. Park J, Maltzahn G, Zhang LL, et al. Magnetic iron oxide nanoworms for tumor targeting and imaging. *Adv Mater*. 2008;20(9):1630–1635. doi:10.1002/adma.200800004

16. Barua Y, Kolhar JW, Wakankar P, Gokarn A, Mitragotri RY, Mitragotri S. Particle shape enhances specificity of antibody-displaying nanoparticles. *Proc Natl Acad Sci U S A*. 2013;110(9):3270–3275. doi:10.1073/pnas.1216893110

17. Wilhelm S, Tavares JA, Dai Q, et al. Analysis of nanoparticle delivery to tumours. *Nat Rev Mater*. 2016;1(5):1–12. doi:10.1038/natrevmats.2016.14

18. Lee SY, Ferrari M, Decuzzi P. Shaping nano-/micro-particles for enhanced vascular interaction in laminar flows. *Nanotechnology*. 2009;20 (49):1–11. doi:10.1088/0957-4484/20/49/495101

19. Adriani G, Tullio MD, Ferrari M, et al. The preferential targeting of the diseased microvasculature by disk-like particles. *Biomaterials*. 2012;33 (22):5504–5513. doi:10.1016/j.biomaterials.2012.04.027

20. Jin Y, Wu ZM, Wu CC, et al. Size-adaptable and ligand (biotin)-sheddable nanocarriers equipped with avidin scavenging technology for deep tumor penetration and reduced toxicity. *J Control Release*. 2020;320:142–158. doi:10.1016/j.jconrel.2020.01.040

21. Yu WQ, Liu R, Zhou Y, Gao HL. Size-tunable strategies for a tumor targeted drug delivery system. *ACS Cent Sci*. 2020;6(2):100–116. doi:10.1021/acscentsci.9b01139

22. Brown MJ, Wilson RW. Exploiting tumour hypoxia in cancer treatment. *Nat Rev Cancer*. 2004;4(6):437–447. doi:10.1038/nrc1367

23. Shim SM, Xia YN. A reactive oxygen species (ROS)-responsive polymer for safe, efficient, and targeted gene delivery in cancer cells. *Angew Chem Int Ed Engl*. 2013;52(27):6926–6929. doi:10.1002/anie.201209633

24. Zhang WL, Wang ZY, Wu CC, et al. The effect of DSPE-PEG2000, cholesterol and drug incorporated in bilayer on the formation of discoidal micelles. *Eur J Pharm Sci*. 2018;125:74–85. doi:10.1016/j.ejps.2018.09.013

25. Diop-Frimpong B, Chauhan PV, Krane S, Boucher Y, Jain KR. Losartan inhibits collagen I synthesis and improves the distribution and efficacy of nanotherapeutics in tumors. *Proc Natl Acad Sci U S A*. 2011;108(7):2909–2914. doi:10.1073/pnas.1018892108

26. Zhang L, Wang Y, Yang Y, et al. High tumor penetration of paclitaxel loaded ph sensitive cleavable liposomes by depletion of tumor collagen I in breast cancer. *ACS Appl Mater Interfaces*. 2015;7(18):9691–9701. doi:10.1021/acsami.5b01473

27. Tang Y, Liu Y, Wang S, et al. Depletion of collagen by losartan to improve tumor accumulation and therapeutic efficacy of photodynamic nanoplatforms. *Drug Deliv Transl Res*. 2019;9(3):615–624. doi:10.1007/s13346-018-00610-1

28. Xia T, He Q, Shi KR, et al. Losartan loaded liposomes improve the antitumor efficacy of liposomal paclitaxel modified with pH sensitive peptides by inhibition of collagen in breast cancer. *Pharm Dev Technol*. 2018;23(1):13–21. doi:10.1080/10837450.2016.1265553

29. Jabir SM, Nayef MU, Abdulkadhim KW, et al. Fe3O4 nanoparticles capped with PEG induce apoptosis in breast cancer AMJ13 cells via mitochondrial damage and reduction of NF-κB translocation. *J Inorg Organomet Polym*. 2021;31:1241–1259. doi:10.1007/s10904-020-01791-4

30. Salman AI, Jabir TE, Sulaiman M, et al. 2-Benzhydrylsulfinyl N hydroxyacetamide Na extracted from fig as a novel cytotoxic and apoptosis inducer in SKOV 3 and AMJ 13 cell lines via P53 and caspase 8 pathway. *Eur Food Res Technol*. 2020;246(8):1591–1608. doi:10.1007/s00217-020-03515-x

31. Ziaydi AI, AI-Shammari GA, Hamzah MA, Kadhim IM, Jabir SH. Newcastle disease virus suppress glycolysis pathway and induce breast cancer cells death. *Virus Dis*. 2020;31(3):341–348. doi:10.1007/s13337-020-00612-z

32. Durymanov OM, Rosenkranz AA, Sobolev SA. Current approaches for improving intratumoral accumulation and distribution of nanomedicines. *Theranostics*. 2015;5(9):1007–1020. doi:10.7150/thno.11742

33. Maeda H. Toward a full understanding of the EPR effect in primary and metastatic tumors as well as issues related to its heterogeneity. *Adv Drug Deliv Rev*. 2015;91:3–6. doi:10.1016/j.addr.2015.01.002

34. Agarwal R, Jurney P, Raythatha M, et al. Effect of shape, size, and aspect ratio on nanoparticle penetration and distribution inside solid tissues using 3D spheroid models. *Adv Healthc Mater*. 2015;4(15):2269–2280. doi:10.1002/adhm.201500441

35. Jin S, Ma XW, Ma HL, et al. Surface chemistry-mediated penetration and gold nanorod thermotherapy in multicellular tumor spheroids. *Nanoscale*. 2013;5(1):143–146. doi:10.1039/C2NR31877F

36. Wang HX, Zou ZQ, Du JZ, et al. Surface charge critically affects tumor penetration and therapeutic efficacy of cancer nanomedicines. *Nano Today*. 2016;11(2):133–144. doi:10.1016/j.nantod.2016.04.008

37. Younus A, Al-Ahmer S, Jabir M. Evaluation of some immunological markers in children with bacterial meningitis caused by Streptococcus pneumoniae. *Res J Biotechnol*. 2019;14(1):131–133.

38. Chen C, Constantinou A, Deonarain M. Modulating antibody pharmacokinetics using hydrophilic polymers. *Expert Opin Drug Deliv*. 2011;8 (9):1221–1236. doi:10.1517/17425247.2011.602399

39. Oddone N, Pederzoli F, Duskey TJ, et al. ROS-responsive "smart" polymeric conjugate: synthesis, characterization and proof-of-concept study. *Int J Pharm*. 2019;570:118655. doi:10.1016/j.ijpharm.2019.118655

40. Shi SR, Zhang LY, Zhu MQ, et al. Reactive oxygen species-responsive nanoparticles based on peglated prodrug for targeted treatment of oral tongue squamous cell carcinoma by combining photodynamic therapy and chemotherapy. *ACS Appl Mater Interfaces*. 2018;10(35):29260–29272.